Electrical Power and Energy Systems 170 (2025) 110895

Contents lists available at ScienceDirect

International Journal of Electrical Power and Energy Systems

journal homepage: www.elsevier.com/locate/ijepes

Consensus control for multi-heterogeneous energy storage system voltage recovery

Tuohan Xiao [a], Don Gamage [a], Chathura Wanigasekara [b], Akshya Swain [a,*], Abhishek Ukil [a]

[a] The University of Auckland, Department of Electrical, Computer, and Software Engineering, Auckland, 1023, New Zealand
[b] German Aerospace Center, Institute of Maritime Energy Systems, Geesthacht, 21502, Germany

ARTICLE INFO

Keywords:
Heterogeneous energy storage systems
Secondary voltage recovery
Droop control
Consensus algorithm
Multi-agent systems

ABSTRACT

The present study proposes a multi-agent framework with a consensus-based secondary voltage recovery (SVR) controller for distributed heterogeneous energy storage systems (HESSs) with different parameters in a DC microgrid. This controller combines the SVR strategy with the virtual resistance/capacitor droop (VRD/VCD) control technique. The SVR control employs a consensus-based approach to balance the state of charge (SoC), power, and energy across multiple HESSs to regulate the DC bus voltage despite load variations and reduce the fluctuation caused by short-circuit current and signal delay. Simulations show the effectiveness of SVR control in recovery and synchronization.

1. Introduction

Due to the scarcity of fossil fuel and environmental concerns, renewable energy deployment is advancing rapidly, including photovoltaic systems, which are widely adopted due to their efficiency [1,2]. Further, in recent years, the integration of distributed generation (DG), energy storage (ES), inverters, protection devices, and localized loads in microgrids has gained significant attention [3]. Most existing microgrids are AC and, therefore, have inherent issues related to frequency regulation, synchronization complexities, and reactive power losses [4]. These challenges are particularly pronounced in the context of distributed renewable energy systems, where DC generation and ES systems dominate [5].

In traditional AC microgrids, DC power from renewable sources and energy storage systems (e.g., batteries) must be converted via DC/AC inverters, leading to energy losses (efficiency reductions of around 12%–18% without DC infrastructure [6]) and increased system complexity. By contrast, DC microgrids (DC MGs) eliminate these conversion steps, enabling direct integration of decentralized DC generators and storage systems to enhance overall efficiency [7,8].

However, despite the advantages of DC MGs, critical challenges persist in three key areas: voltage regulation, distributed coordination, and control system reliability [9]. Due to its intermittent nature, large-scale PV integration introduces severe voltage fluctuations that traditional ES-based stabilization methods struggle to address promptly [10]. Meanwhile, decentralized consensus algorithms, although promising for coordinating multi-battery systems, suffer from long convergence times and are sensitive to communication delays, resulting in inconsistent operation of energy storage units [11]. Additionally, secondary voltage recovery (SVR)-based control techniques, designed to regulate power and voltage, often encounter problems such as supercapacitor current leakage and voltage instability caused by data transmission delays [12]. These issues highlight the urgent need for a more comprehensive and robust control solution.

Over the past decades, researchers have explored various strategies to tackle these problems. For example, studies like [11] have investigated decentralized synchronization in uncertain networks, focusing on subsystem interactions, while [13] has shown that frequent communication can enhance transient responses in subsystems. Additionally, [14] introduced extended droop control methods for better power management of batteries and supercapacitors.

In parallel, consensus algorithms have gained attraction in engineering, especially in modern smart grids with renewable energy integration. Distributed consensus algorithms enable converter units to optimize control strategies collaboratively by exchanging information, thereby enhancing system flexibility [15,16]. Researchers have also proposed consensus-based algorithms for coordinating battery energy storage systems in a fully distributed manner [17] and for managing power fluctuations from loads and renewable sources [18]. Nevertheless, most existing SVR-based control techniques still have significant drawbacks. For instance, the SVR control proposed in [12] is unstable

* Corresponding author.
E-mail addresses: txia520@aucklanduni.ac.nz (T. Xiao), dgam963@aucklanduni.ac.nz (D. Gamage), chathura.wanigasekara@dlr.de (C. Wanigasekara), a.swain@auckland.ac.nz (A. Swain), a.ukil@auckland.ac.nz (A. Ukil).

https://doi.org/10.1016/j.ijepes.2025.110895
Received 28 April 2025; Received in revised form 22 June 2025; Accepted 8 July 2025

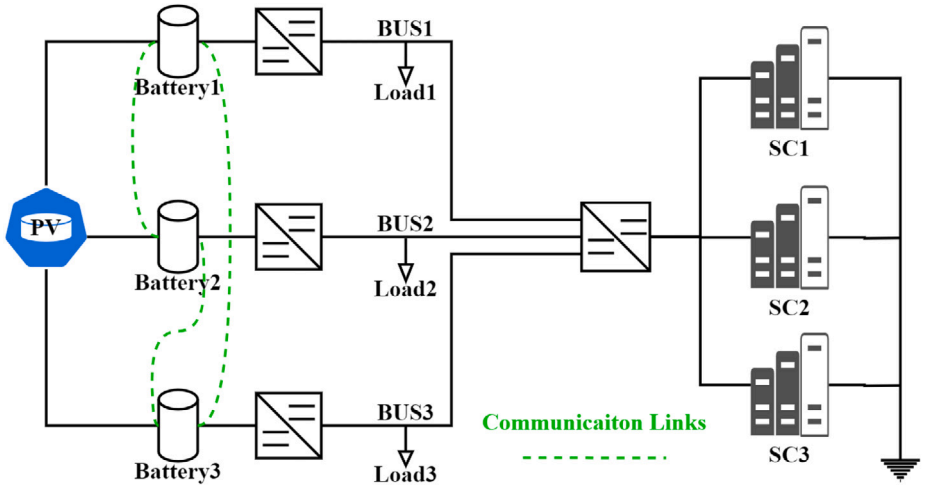

Fig. 1. Structure of an interconnected distributed DC MG.

due to supercapacitor current leakage, and the methods in [19,20] suffer from voltage variations caused by data delay-induced system imbalances.

By taking these aspects into consideration, the present study aims to bridge these gaps by treating the DC microgrid system as a multi-agent framework with fully connected bidirectional synchronous communication. We propose a modified SVR-based primary virtual/impedance droop control technique integrated with consensus control. This novel approach, as illustrated in Fig. 1, addresses traditional issues of slow response, inefficient coordination, and communication sensitivity by integrating SVR-based virtual impedance droop control for real-time voltage fluctuation compensation with consensus control via fully connected synchronous communication to enable rapid power/SoC consensus across multi-agents.

The following are the main contributions of this study.

i. An advanced SVR controller for the HESS hierarchy system is proposed to effectively stabilize the bus voltage for systems with PV integration, considering the system as a multi-agent system.
ii. The proposed controller ensures power and energy consensus among all batteries in a DC microgrid with SC.
iii. This method converges all SoCs for every agent and validates the correctness of the relationship between SoC and power.
iv. The control strategy ensures system stability across diverse signal conditions, including intentional delays and packet loss.

The remainder of this paper is structured as follows: Section 2 describes the architecture of the multi-agent system and the relevant knowledge of the consensus algorithm is introduced in Section 3. Details of each system function and relevant parameters are described in Section 5 and system stability is analysed with respect to parameter values in Section 5. Effectives of the proposed controller using numerical simulations are investigated in Section 6 and concluding remarks are given in Section 7.

2. System description

The block diagram of the power management system, considered in this study, is shown in Fig. 2. The power generated by the PV renewable energy source is combined with the battery to supply the load via a bidirectional DC/DC converter, which ensures that the voltage on the DC bus remains stable during battery charging/discharging operations. Furthermore, any variations in the power output from the PV source trigger a dynamic recovery process, and the corresponding system response is explicitly reflected in the voltage profile of the DC bus. The supercapacitors are connected to the load via a converter that assists

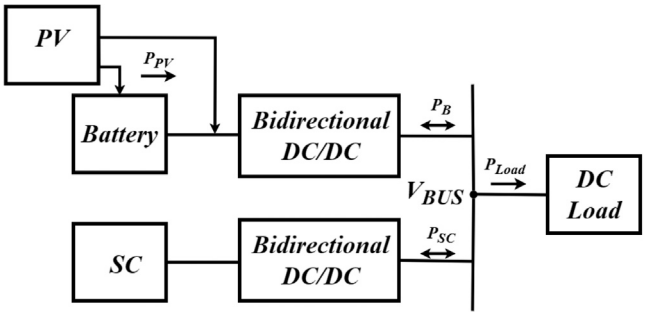

Fig. 2. Schematic diagram of power management.

with frequency regulation. The SoC is regulated to avoid boundary violations. In this study, a decentralized power management model for parallel energy storage systems is proposed for proportionate power distribution.

2.1. Traditional droop control techniques for transient power sharing

Since, the goal is to design a modified SVR based on a traditional droop controller, it is appropriate to discuss first some key features of droop controller. Fig. 3 shows the schematic of a droop control system with VRD and VCD controller of a typical HESS (say ith HESS) used in PV system consisting of both a battery and a supercapacitor. The battery is modelled as a DC source in series with a virtual resistance R_V and the supercapacitor is represented by a battery in series with a virtual capacitor C_V. From Fig. 3, the voltage current relation of battery converters for ith HESS is given by:

$$v_{oBi} = v_{ref} - R_V i_{oBi} \tag{1}$$

where v_{oBi} is the ith output voltage, i_{oBi} is the ith output current of the battery converter, v_{ref} is the bus voltage reference, and R_V is the virtual droop resistance.

The voltage current relation of supercapacitors for ith HESS is:

$$v_{oSCi} = v_{ref} - \frac{1}{sC_V} i_{oSCi} \tag{2}$$

where v_{oSCi} is the ith output voltage, i_{oSCi} is its ith output current and C_V is the virtual droop capacitor.

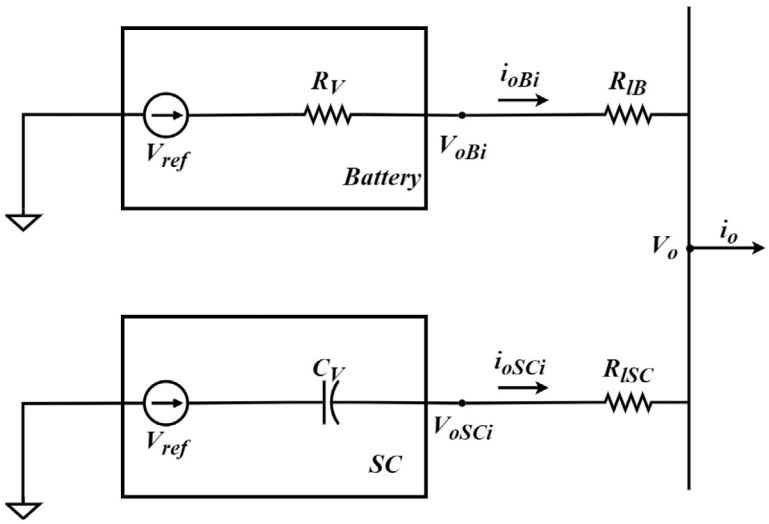

Fig. 3. Equivalent circuit for traditional droop controller.

From Fig. 3, $i_{oi} = i_{oBi} + i_{oSCi}$ where,

$$\begin{cases} i_{oBi} = \dfrac{Z_{SC}}{Z_{SC}+Z_B} i_{oi} \\ i_{oSCi} = \dfrac{Z_B}{Z_{SC}+Z_B} i_{oi} \\ Z_B = R_V \\ Z_{SC} = \dfrac{1}{sC_V} \end{cases} \tag{3}$$

Here, Z_B, Z_{SC} are the virtual impedance of the battery and SC, respectively. Note that VCD and VRD controllers can accomplish power-sharing of ESs with varying dynamics using the above relation. Further, the load current can be split into high-frequency and low-frequency components, which are assigned to the SC and battery, respectively, and the crossover frequency is $\omega = \dfrac{1}{R_V C_V}$. This leverages their complementary traits for efficient power sharing. Although, the droop control strategy can achieve successful power allocation, its performance degrades with variations in bus voltage and it is often impossible to rapidly recover the SC's terminal voltage after charging or discharging.

2.2. Hierarchical control and SoC state analysis

To overcome the limitations of the traditional droop controller in VRD and VCD control, a hierarchical control strategy is proposed. The block diagrams of the proposed control method are shown in Fig. 4, which shows the basic structure of HESS, and Fig. 5, which comprises two loops: an external voltage loop and an inner current loop. According to Fig. 5, the VRD controller stabilizes the battery voltage (v_{oB}), while the VCD controller is designed to quickly restore the SC terminal voltage (v_{SC}) after charging or discharging. The SVR control minimizes the DC bus voltage deviation and compensates for the SC current caused by load and demand. Consensus control prevents the circuit loop current (i_{LB}) from fluctuating due to PV power changes.

The output of SVR control of the battery can be expressed as:

$$\theta_{VB}(t) = k_{PB} e_{oB}(t) + k_{IB} \int e_{oB}(t) dt \tag{4}$$

where $e_{oB}(t) = v_{ref}(t) - v_{oB}(t)$ is the mismatch between v_{oB} and reference voltage, k_{IB} and k_{PB} are the parameters of battery controller $C_B(t)$.

Since the primary control responds fast, its dynamics can be ignored while analysing the secondary control. The output of the battery with the inclusion of secondary control is given by:

$$v_{oB}(t) = v_{ref}(t) + \theta_{VB}(t) - R_V i_{oB}(t) = v^*_{oB}(t) \tag{5}$$

The output of SC terminal voltage is time-varying and can be expressed as:

$$v_{SC}(t) = v_{SC}(t_0) - \frac{1}{C_{SC}} \int_{t_0}^{t} \left[i_{LSC}(t) + \frac{v_{SC}(t)}{R_{SC}} \right] dt \tag{6}$$

where C_{SC} and R_{SC} denote the capacitance and resistance of SC respectively. The terminal voltage of SC terminal at time t_0, is denoted by $v_{SC}(t_0)$ and equals to v_{SCN}, in this study.

The output of the SVR control of SC is:

$$\theta_{ISC}(t) = k_{PSC} e_{SC} + k_{ISC} \int e_{SC} dt \tag{7}$$

where $e_{SC} = v_{ref} - v_{SC}(t)$; v_{SC} is the terminal voltage of the SC and k_{PSC} and k_{ISC} are the gains of the PI controller C_{sc}.

As shown in Fig. 6, when the PV source is added to the system, it impacts the charge state of the battery and causes current fluctuations. To minimize the difference between the operating current and the stable state current of the loop current i_{LB}, using $P_B = V_B I_B$ to determine the reference current $i_{Bat.ref}$ through a consensus controller. Due to the rapid response of the internal current control loop, the current flowing through the battery converter ideally matches this reference value. Therefore, the transfer function can be considered as 1. The current of the battery converter is computed from the following:

$$\begin{aligned} i_{LB} = & i_{PV} - i_{Bat.ref} + k_{PV\_B} \left(e_{oB} + \theta_{VB} - R_V D_B i_{LB} \right) \\ & + \; k_{IV\_B} \int \left(e_{oB} + \theta_{VB} - R_V D_B i_{LB} \right) dt \end{aligned} \tag{8}$$

where D_B is the nominal duty ratio of the battery converter and k_{PV_B}, and k_{IV_B} are the proportional and integral gains of the voltage control loop.

The current through the battery i_B is given by:

$$\begin{aligned} i_B &= i_{PV} - i_{LB} \\ &= i_{Bat.ref} - (k_{PV\_B} \left[e_{oB} + \theta_{VB} - R_V D_B i_{LB} \right) \\ &+ \; k_{IV\_B} \int \left(e_{oB} + \theta_{VB} - R_V D_B i_{LB} \right) dt] \end{aligned} \tag{9}$$

The system is stabilized by charging or discharging of the battery depending on the load demand. At stabilization, i_B will be equal to zero. The dynamics of state of charge of battery at time t is expressed as:

$$SoC(t) = SoC(t_0) - \frac{1}{C_B} \int_{t_0}^{t} i_B(\tau)\, d\tau \tag{10}$$

where C_B is the capacitor of battery, and $SoC(t_0)$ represents the initial SoC state.

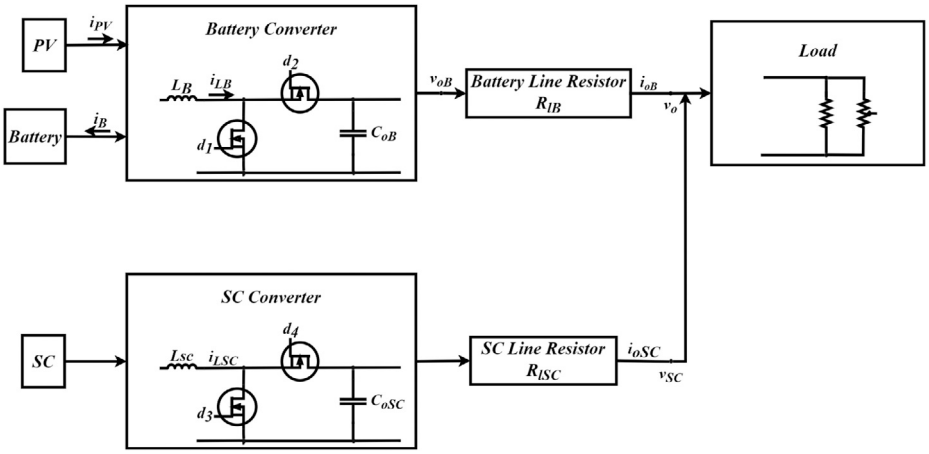

Fig. 4. Battery and SC structure of HESS.

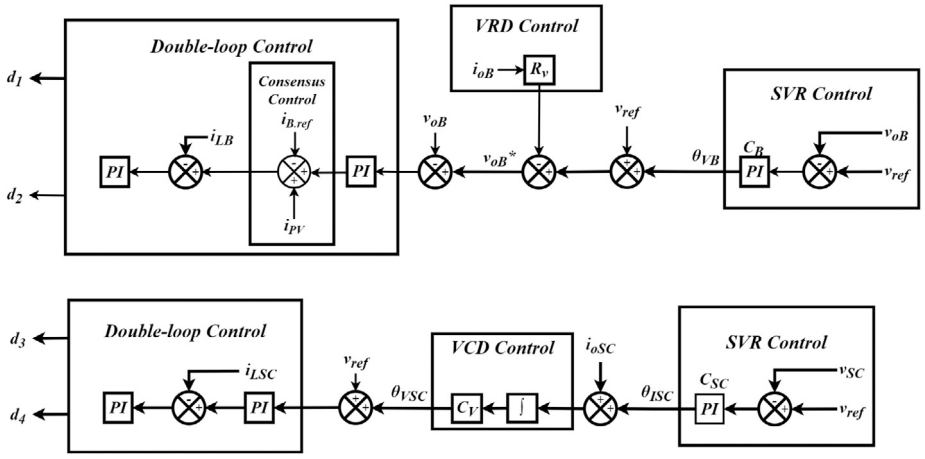

Fig. 5. Converter controls of HESS.

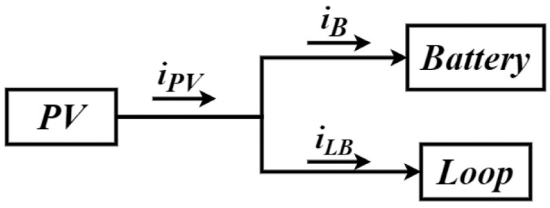

Fig. 6. Current distribution.

The parameters of the system, investigated in this study, are shown in Table 1.

The gains of the controllers are taken from [4] and are shown in Table 2.

To expand the system from a single agent to multiple agents, a Power/Energy-based consensus controller is introduced under the assumption of fully connected bidirectional synchronous communication. This communication topology ensures that each agent can directly exchange information with all others without delay, enabling real-time synchronization of control signals. The controller sets the reference current ($i_{Bat.ref\,i}$) for each battery circuit loop, as shown in Fig. 7, which is obtained from battery current i_B through consensus control. Finally, the input of each MOSFET of the HESS converter di is generated.

From (10),

$$\dot{S}oC_i(t) = -I_{B_i}/C_{oB} \tag{11}$$

Table 1
System relevant parameters.

Parameters	Description	Values
V_{ref}	DC bus reference voltage	48 V
V_{nom1}	Nominal voltage of battery (charging)	45 V
V_{nom2}	Nominal voltage of battery (discharging)	43 V
R_{load}	Load impedance	25 Ω
R_{line}	Line impedance	0.02 Ω
R_V	Virtual resistance	0.1 Ω
C_V	Virtual capacitor	0.02 Ω
C_{SC}	capacitor of SC	2.5 F
C_B	capacitor of battery	9 F
L_B/L_{SC}	Filter inductance of converters	0.0008 H
C_{oB}/C_{oSC}	Filter capacitor of converters	0.006 F

Hence, the output discharge/charge power ΔP_{B_i} of the ith battery can be calculated using the formula $\Delta P_{B_i} = V_{B_i} I_{B_i}$. The output battery voltage V_{B_i} for $i = 1, \ldots, n$ remains unchanged throughout a wide range of SoC. Therefore, $\dot{S}oC_i(t)$ is formulated as:

$$\dot{S}oC_i(t) = -\frac{\Delta P_{B_i}}{C_{oB} V_{Bi}}, \quad i = 1, \ldots, n. \tag{12}$$

Power is linked to the first-order derivative of SoC, ensuring stable state after discharge/charge of battery current. This method further regulates $d_1, d_2, d_5, d_6, d_9, d_{10}$ and final output voltage. $SoC_i(t)$ is expressed

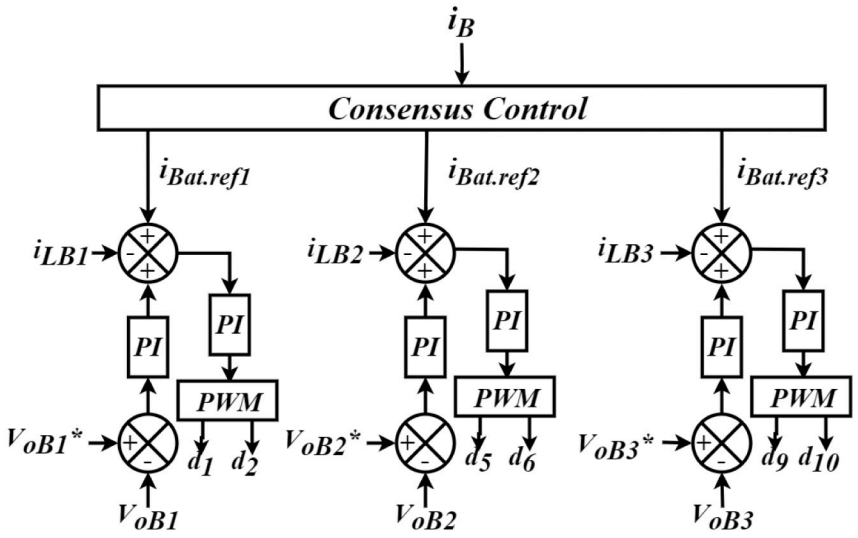

(a) PWM rectification for multi-battery.

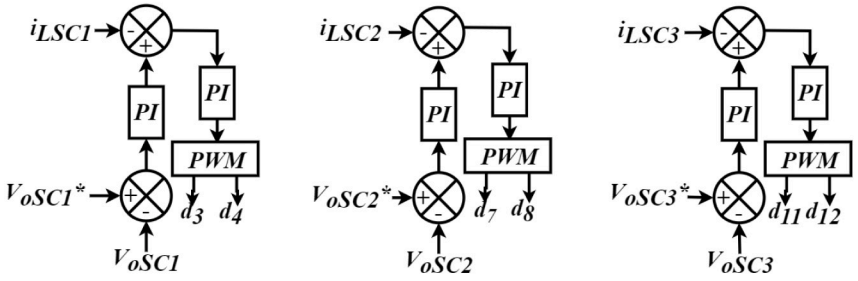

(b) PWM rectification for multi-SC.

Fig. 7. Consensus algorithm control system block diagram.

Table 2
PID controller parameters.

Parameters	Description	Values
k_{PB}	Battery secondary controller	0.3
k_{IB}	Battery secondary controller	0.5
k_{PSC}	SC secondary controller	0.3
k_{ISC}	SC secondary controller	0.05
k_{PV_B}	Battery voltage loop controller	2
k_{IV_B}	Battery voltage loop controller	50
k_{PV_SC}	SC voltage loop controller	50
k_{IV_SC}	SC voltage loop controller	50
k_{PC_i}	Current loop controller	0.008
k_{IC_i}	Current loop controller	2.5

as:

$$SoC_i(t) = SoC_i(t_0) - \frac{E_{B_i}}{C_{oB}V_{B_i}}, \quad i = 1, \ldots, n. \tag{13}$$

In this paper, we confine the region of $10\% < SoC_{mini} < 20\%$ and $90\% < SoC_{maxi} < 100\%$, to avoid excessive charging and discharging, which can significantly accelerate battery aging [21,22]. For supercapacitors, it prevents the 15% capacitance fade and 50% internal resistance growth caused by full-charge storage (SoC = 100%), ensuring less than 20% capacitance decay over 10,000 cycles. This SoC management balances energy efficiency with component longevity, enhancing the long-term effectiveness of control strategies by systematically addressing age-related performance degradation [23,24]. Therefore,

$$SoC_{mini} < SoC_{bat,ti} < SoC_{maxi}. \tag{14}$$

3. Multiple agent consensus algorithm theory

In the present study, the control problem is addressed using a multi-agent framework where each HESS is considered as an agent. Since this framework uses graph theory, we briefly discuss this for easy reference.

Consider a system with n-number of HESS units, where each unit communicates with others through a network. This communication structure can be represented as a graph $G = (\Delta, \Gamma)$, where $\Delta = [\Delta_1, \Delta_2, \ldots, \Delta_n]$ denotes the nodes (corresponding to agents), and $\Gamma = (i, j)$ defines the set of edges that connect these nodes. Here, $j \in N_i$ indicates the neighbouring nodes of i. The adjacency matrix $A_d = [a_{ij}]$, an $n \times n$ matrix, reflects whether any two nodes in the network are connected [25]. The adjacency matrix $A_d = [a_{ij}]$ of the graph G is defined as:

$$a_{ij} = \begin{cases} 1 & \text{if there is an edge from node } v_i \text{ to node } v_j, \\ 0 & \text{otherwise.} \end{cases} \tag{15}$$

Each diagonal a component d_{ij} in the degree matrix D represents the degree of a node v_i:

$$d_{ij} = \begin{cases} \sum_{j=1}^{n} a_{ij} & \text{if } i = j \\ 0 & \text{if } i \neq j. \end{cases} \tag{16}$$

The Laplacian matrix L is a positive semi-definite matrix with non-negative real eigenvalues, defined as:

$$L = D - A \tag{17}$$

4. Problem formulation

Consider a networked system consisting of multiple nodes, where the state of each node is described by:

$$\dot{x}_i(t) = Ax_i(t) + Bu_i(t)$$
$$y(t) = Cx_i(t) \tag{18}$$

Building on the state function defined in (18), this formulation serves to characterize the dynamic interactions among networked nodes, laying the foundation for subsequent control design. The objective is to design a consensus controller to balance the current of the battery circuit loop by optimizing the following function at each agent.

$$J_i = \int_0^\infty \left(x_i(t)^\mathcal{T} Q x_i(t) + u_i(t)^\mathcal{T} R u_i(t) \right) dt \tag{19}$$

where $Q \geq 0$ is the state weighting matrix, $R > 0$ is the control weighting matrix.

The total system cost function is the sum of cost functions of all agents:

$$J = \sum_i J_i = \sum_i \int_0^\infty \left(x_i(t)^\mathcal{T} Q x_i(t) + u_i(t)^\mathcal{T} R u_i(t) \right) dt \tag{20}$$

The optimal control strategy, for each agent, is obtained using Hamilton–Jacobi–Bellman (HJB) equation assuming Lyapunov function $V_i(x_i) = x_i P x_i^\mathcal{T}$. The HJB equation for each agent i is given by:

$$\begin{aligned} \frac{dV_i}{dt} &= \min_{u_i} \left(x_i^\mathcal{T} Q x_i + u_i^\mathcal{T} R u_i + \frac{\partial V_i}{\partial x_i} \cdot \dot{x}_i \right) \\ &= \min_{u_i} \left(x_i^\mathcal{T} Q x_i + u_i^\mathcal{T} R u_i + \frac{\partial V_i}{\partial x_i} (Ax_i(t) + Bu_i(t)) \right) \end{aligned} \tag{21}$$

Taking the derivative with respect to u_i and setting it to zero, gives the optimal control law:

$$\begin{aligned} &\frac{\partial}{\partial u_i} \left(u_i^\mathcal{T} R u_i + \frac{\partial V_i}{\partial x_i} B u_i \right) = 0 \\ &u_i^* = -R^{-1} B^\mathcal{T} \frac{\partial V_i}{\partial x_i} \end{aligned} \tag{22}$$

Substituting the optimal control law u_i^* into the HJB equation, we obtain the following form:

$$\begin{aligned} \frac{dV_i}{dt} &= x_i^\mathcal{T} Q x_i + x_i^\mathcal{T} P_i A x_i + x_i^\mathcal{T} A^\mathcal{T} P_i x_i \\ &\quad - x_i^\mathcal{T} P_i B R^{-1} B^\mathcal{T} P_i x_i \end{aligned} \tag{23}$$

The Riccati equation for each agent i is given by:

$$A^\mathcal{T} P_i + P_i A - P_i B R^{-1} B^\mathcal{T} P_i + Q = 0 \tag{24}$$

Solving this Riccati equation gives the matrix P_i, which can then be used to compute the optimal feedback gain K and is given by:

$$K = R^{-1} B^\mathcal{T} P_i \tag{25}$$

The control input $u_i(t)$, for each node is selected as:

$$u_i(t) = cK \sum_j a_{ij}(x_j(t) - x_i(t)) \tag{26}$$

where c is a design parameter to ensure stability. Substituting the control input into the state equation gives:

$$\dot{x}_i(t) = Ax_i(t) + B \left(cK \sum_j a_{ij}(x_j(t) - x_i(t)) \right) \tag{27}$$

where a_{ij} is the weight of the connection from node j to node i, $x_i(t)$ is the state of the ith node. A is the system matrix. B is the input matrix. The matrix C denotes the output matrix. K is the gain matrix obtained by optimizing the quadratic cost function J_i, and c is the scalar gain that is selected to ensure stability.

5. Stability analysis

To choose the value of each matrix and gains, the Lyapunov function $V(x) = xPx^\mathcal{T}$ needs to meet the following requirement according to the Lyapunov Stability principle:

$$\dot{V}(x) < 0 \tag{28}$$

Considering the entire system state vector $x = \begin{pmatrix} x_1 \\ x_2 \\ \vdots \\ x_N \end{pmatrix}$ the system can be represented as:

$$\dot{x}(t) = (I_N \otimes A)x(t) + (I_N \otimes B)u(t) \tag{29}$$

where $u(t)$ is the vector of all control inputs.

$$u(t) = -c(L \otimes K)x(t) \tag{30}$$

where K is the gain matrix, L is Laplacian matrix.

Substituting $u(t)$, the closed loop system becomes:

$$\begin{aligned} \dot{x}(t) &= (I_N \otimes A - c(I_N \otimes B)(L \otimes K))x(t) \\ &= [I_N \otimes A - c(L \otimes BK)]x(t) \end{aligned} \tag{31}$$

In order to investigate the stability of the system, consider a Lyapunov function:

$$V(x) = x^\mathcal{T}(I_N \otimes P)x \tag{32}$$

The time derivative of the Lyapunov function is computed as follows:

$$\begin{aligned} \dot{V}(x) &= \frac{d}{dt}(x^\mathcal{T}(I_N \otimes P)x) \\ &= \dot{x}^\mathcal{T}(I_N \otimes P)x + x^\mathcal{T}(I_N \otimes P)\dot{x} \\ &= \left((I_N \otimes A - c(L \otimes BK))x\right)^\mathcal{T}(I_N \otimes P)x \\ &\quad + x^\mathcal{T}(I_N \otimes P)\left((I_N \otimes A - c(L \otimes BK))x\right) \end{aligned} \tag{33}$$

This can further be simplified as:

$$\begin{aligned} \dot{V}(x) &= x^\mathcal{T}\Big((I_N \otimes A - c(L \otimes BK))^\mathcal{T}(I_N \otimes P) \\ &\quad + (I_N \otimes P)(I_N \otimes A - c(L \otimes BK))\Big)x \\ &= x^\mathcal{T}\Big((I_N \otimes A^\mathcal{T} - c(L \otimes BK)^\mathcal{T})(I_N \otimes P) \\ &\quad + (I_N \otimes P)(I_N \otimes A - c(L \otimes BK))\Big)x \\ &= x^\mathcal{T}\Big(I_N \otimes (PA + A^\mathcal{T}P) \\ &\quad - c(L \otimes (PBK + K^\mathcal{T}B^\mathcal{T}P))\Big)x \end{aligned} \tag{34}$$

To ensure $\dot{V}(x) < 0$, P, c and K need to satisfy:

$$PA + A^\mathcal{T}P - c(PBK + K^\mathcal{T}B^\mathcal{T}P) < 0 \tag{35}$$

The stability of the closed loop system of (31) is equivalent to the stability of the matrix

$$\left(A - c\lambda_i BK\right) \tag{36}$$

where λ_i is the minimum eigenvalue of the Laplacian. It has been shown in [26] that for the closed loop system to be stable, c must satisfy the following criteria,

$$c \geq \frac{1}{2min_i Re(\lambda_i)} \tag{37}$$

where $min_i Re\lambda_i$ is the real part of the minimum eigenvalue. Since $P > 0$ and $Q > 0$, according to Lyapunov theory in [27], (36) is asymptotically stable if $c \geq 1/2min_i Re(\lambda_i), \forall i \in \mathbb{N}$ [26].

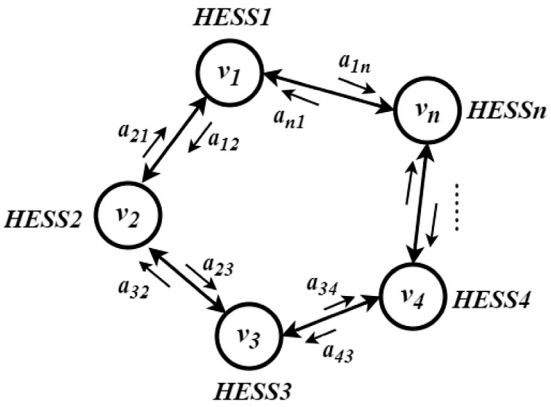

Fig. 8. Bi-directional communication graph.

Table 3
Validation of results.

Controller type	Controller description
Advanced SVR controller	SVR control with VRD/VCD control based on consensus control
Traditional SVR controller	SVR control based on consensus control
Wthout SVR controller	VRD/VCD control based on consensus control
Controller type	**Voltage and Power performance**
Advanced SVR controller	Instantaneous voltage recovery Stable output of DC bus voltage Provide continuous high-level power
Traditional SVR controller	Instantaneous voltage recovery Unstable output of DC bus voltage Only provide 49s high-level power
Wthout SVR controller	Instantaneous voltage recovery Unstable output of DC bus voltage Only provide 45s high-level power

6. Simulation results

The effectiveness of the proposed control framework is investigated considering a 3-node distributed HESS in a DC microgrid shown in Fig. 7. This system can be represented by the bi-directional graph shown in Fig. 8 with $n = 3$ where the three agents can communicate with each other, the Laplacian matrix L is:

$$L = \begin{pmatrix} 2 & -1 & -1 \\ -1 & 2 & -1 \\ -1 & -1 & 2 \end{pmatrix} \tag{38}$$

and its eigenvalues are $\lambda_1(L) = 0,\ \lambda_2(L) = 3,\ \lambda_3(L) = 3$.

The dynamics of ith HESS can be expressed by a linear state space model as [28]:

$$\underbrace{\begin{bmatrix} \dot{E}_i(t) \\ \dot{P}_i(t) \end{bmatrix}}_{\dot{x}_i} = \underbrace{\begin{bmatrix} 0 & -\frac{1}{3600} \\ 0 & 0 \end{bmatrix}}_{A_i} \underbrace{\begin{bmatrix} E_i(t) \\ P_i(t) \end{bmatrix}}_{x_i} + \underbrace{\begin{bmatrix} 0 \\ 1 \end{bmatrix}}_{B_i} u_i(t)$$

$$y_i(t) = \underbrace{\begin{bmatrix} 0 & \frac{1}{V_B} \end{bmatrix}}_{C_i} \begin{bmatrix} E_i(t) \\ P_i(t) \end{bmatrix} \tag{39}$$

The variables E_i and P_i stand for the energy and power levels of the ith battery. Additionally, battery ratings expressed in kilowatt-hours (kWh) and kilowatts (kW) are converted to the appropriate units using a coefficient of $\frac{1}{3600}$. The input of ith agent can be expressed as:

$$\begin{aligned} u_1 &= -c \begin{bmatrix} K_1 & K_2 \end{bmatrix} \begin{bmatrix} 2E_{b_1} - E_{b_2} - E_{b_3} \\ 2P_{b_1} - P_{b_2} - P_{b_3} \end{bmatrix} \\ u_2 &= -c \begin{bmatrix} K_1 & K_2 \end{bmatrix} \begin{bmatrix} -E_{b_1} + 2E_{b_2} - E_{b_3} \\ -P_{b_1} + 2P_{b_2} - P_{b_3} \end{bmatrix} \\ u_3 &= -c \begin{bmatrix} K_1 & K_2 \end{bmatrix} \begin{bmatrix} -E_{b_1} - E_{b_2} + 2E_{b_3} \\ -P_{b_1} - P_{b_2} + 2P_{b_3} \end{bmatrix} \end{aligned} \tag{40}$$

The consensus algorithm parameters are derived by following the procedure in Sections 3 and 4, integrating previously obtained system parameters to ensure stability and convergence, and validated by confirming $\dot{V} < 0$. In this study, the parameter c is selected as 1 and the controller gain matrix $K = [-28.2843 \quad 3.1648]$.

With the proposed consensus control, the power and energy of each battery converged to the same value, as shown in Fig. 9. Note that the lines in the upper half represent energy, and the lower half represent power.

Next, the objective is to investigate if the system could accurately follow the reference SoC generated using (13), both during charging and discharging conditions. Fig. 10 shows that the system could track the reference SoC with maximum of 5% error.

With the consensus controller, the battery current I_B could successfully track the reference as shown in Fig. 12, and there is no need to consider signal delay because of the dynamic inputs of the consensus algorithm. Note that the ability of PV to supply enough power to meet load demands depends on the nominal voltage of the battery. The battery will begin to drain if the load demand exceeds the energy supplied by the P. Otherwise, it will charge to absorb the excess energy. Fig. 11 shows the SoCs when the battery is in the discharging and charging states. The results illustrate that the SoC of each agent can charge or discharge to the same final state from different initial states.

Initially, to validate the effectiveness of an advanced SVR controller, one HESS is used. Note that due to power-sharing, only low frequency goes through the battery, and no high-frequency interference in results. The performance of different controllers is shown in Table 3. The changes in voltages, currents and power are shown in Figs. 13–15. From these figures, it is observed that during 10 s to 20 s, load demands vary due to changes in V_{PV}, causing fluctuations in voltage and current. Finally, we conclude that the advanced SVR control is most effective because it can exhibit minimal voltage fluctuation, maintain high current in the battery and PV loop, and ensure stable, high power to meet bus load demands. This is because the SVR controller and consensus controller adjust output current dynamically to stabilize the voltage while traditional SVR control and without SVR control neglect V_{oB} errors, leading to frequent fluctuations in the recovery period.

Next, the simulations are carried out considering all three agents. The results of advanced SVR are shown in Fig. 16, where it is observed that all three agents can provide stable DC bus voltage and high-level power to meet demand. The currents in the loads are shown in Fig. 17. Due to stable voltage output, these currents exhibit little fluctuations (caused by a drop in load resistance and a drop in V_{PV}) before stabilizing.

Considering the impact of signal loss, Fig. 18 illustrates the entire current recovery process. When the input signal to the MOSFET of Agent 3 is lost between 15s and 20s, the recovery of the agents exhibits distinct oscillations compared to Fig. 17. However, under the coordination provided by the advanced SVR controller, the current eventually recovers to the correct value. Meanwhile, the SoC of Agent 3 exhibits only a slight deviation and ultimately converges to the same value as the other agents (see Fig. 19).

Signal delay scenarios reveal similar behavioural patterns. As shown in Fig. 20, when all input signals to the MOSFETs of Agent 1 are delayed by one sample time, the recovery process of Agent 1 lags behind that of the other agents by 1 s. Despite this initial delay, the current of Agent 1 eventually returns to the expected value. The SOC dynamics under these conditions are presented in Fig. 21. Notably, the SOC of Agent 1 exhibits an accelerated charging phase, actively compensating for the

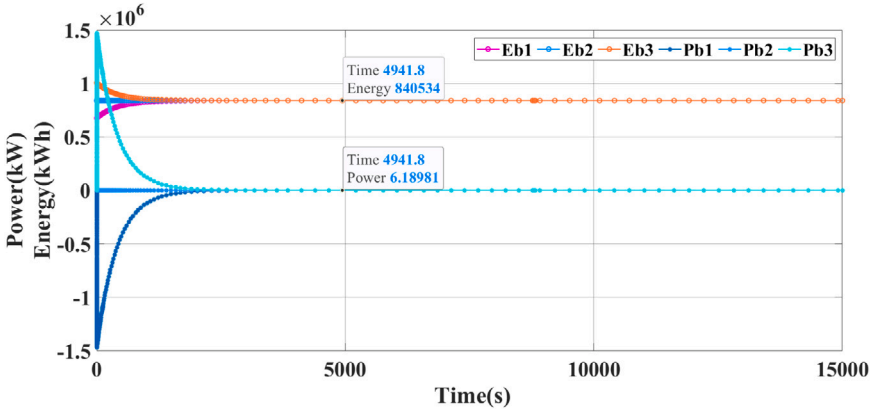

Fig. 9. Convergence of power and energy.

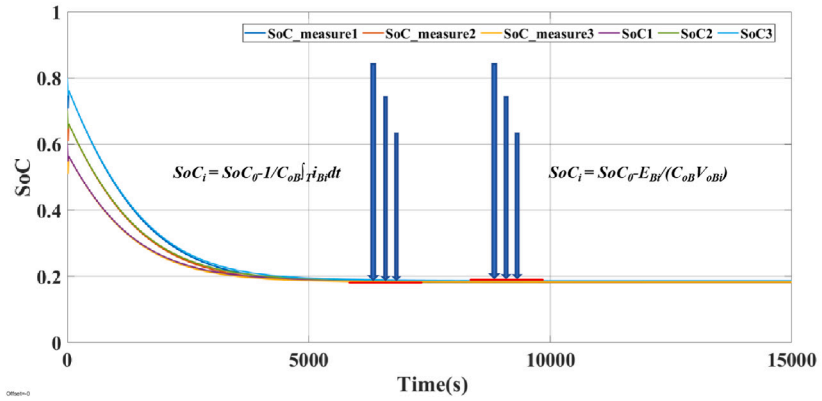

(a) Discharging state.

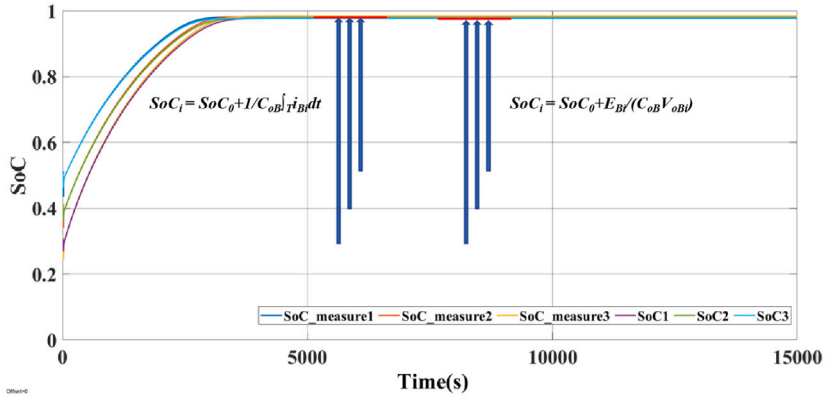

(b) Charging state.

Fig. 10. Comparison of SoC value evaluated by energy and detected in the proposed model.

power imbalance induced by the signal delay to ensure system-wide equilibrium.

A comparison of different communication states is presented in Table 4.

7. Conclusion

For HESSs in DC MGs using a consensus algorithm, this work suggests an advanced SVR control strategy based on virtual VRD control and VCD control. From the above discussion, we can conclude that in a stable system, the output voltage and battery terminal voltage can recover to V_{ref} in a very short time, and that the fast recovery output voltage benefits the current through the loads, which is only affected by the load demand. This is achieved with the assistance of the SVR controller, which is used to analogue the error of V_{oB}, and the auxiliary consensus algorithm, which is used to calculate the error of i_{LB}. Thus, compared with previous work, this method is good at recovery speed and accuracy, and reduces the impact of short-circuit current and signal

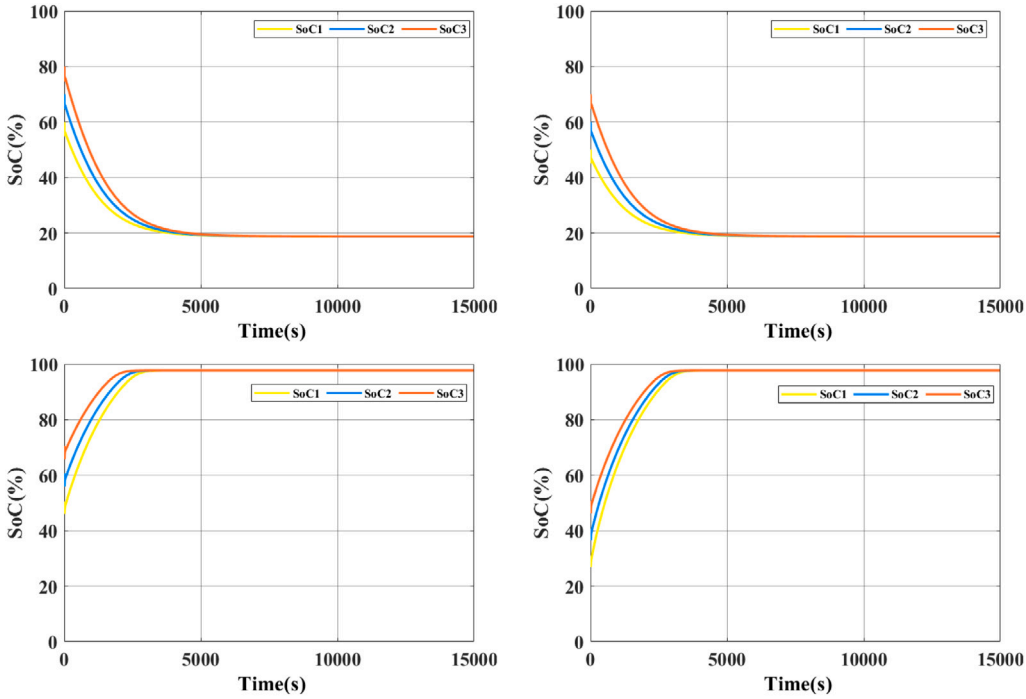

Fig. 11. Batteries discharge/charge from different initial values.

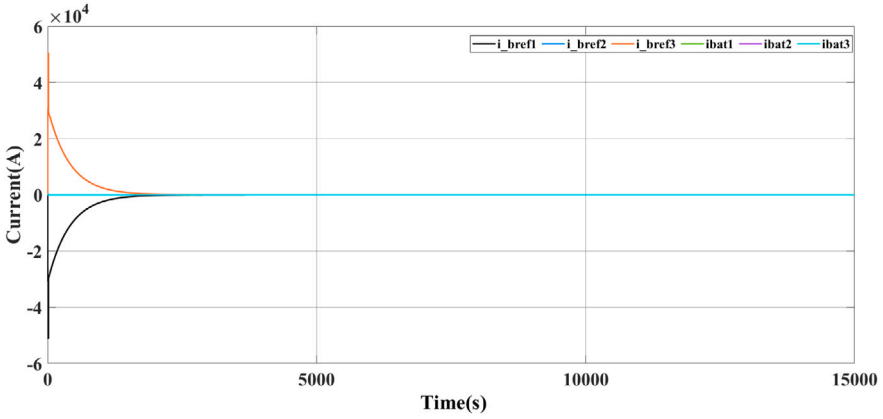

Fig. 12. Convergence of $I_{Bat.ref}$ and I_B.

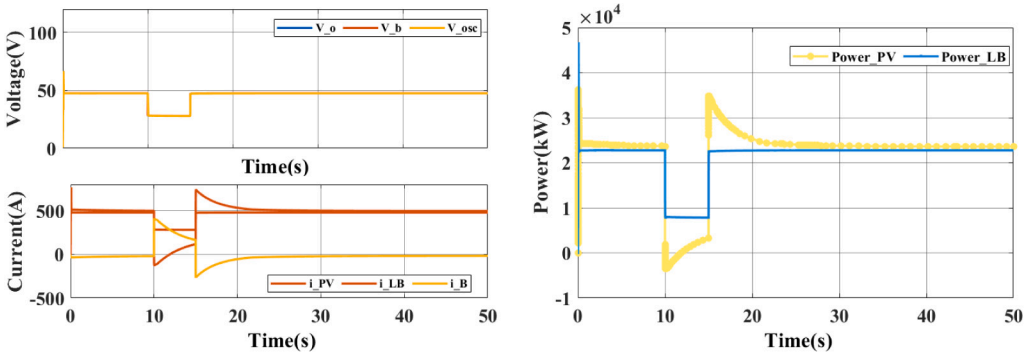

(a) Voltage and current curves. (b) Power curves.

Fig. 13. Voltage, current and power curves under advanced SVR control.

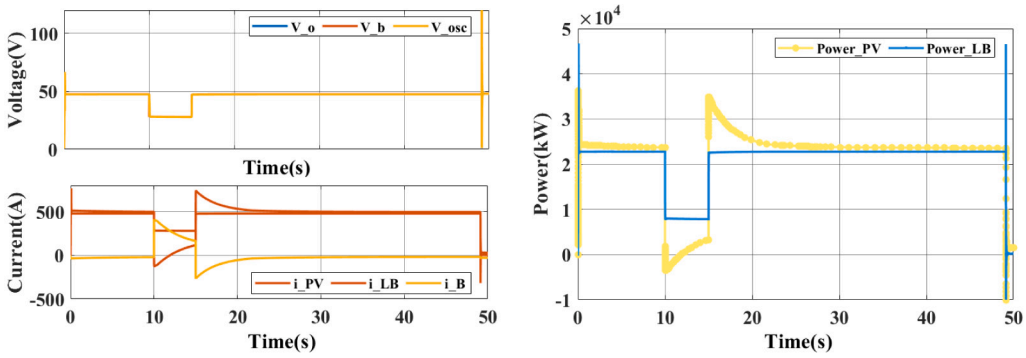

(a) Voltage and current curves. (b) Power curves.

Fig. 14. Voltage, current and power curves under traditional SVR control.

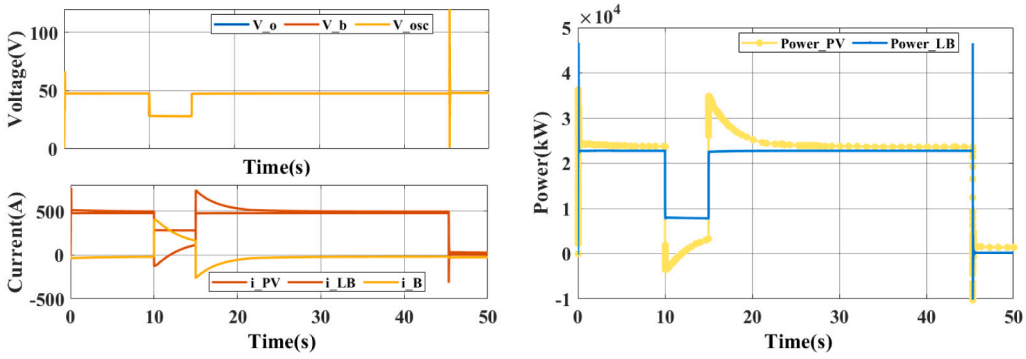

(a) Voltage and current curves. (b) Power curves.

Fig. 15. Voltage, current and power curves without SVR control.

Table 4
System performance under different communication states.

Communication state	Performance
Normal	System can recover to the setting value normally SoC of each agent always maintain consistency
Under signal loss	The output recovery of the affected agent exhibits oscillations The SoC charging of affected agent accelerates SoC of each agent can finally maintain consistency
Under signal delay	The output recovery of the affected agent shows delays The SoC charging of affected agent accelerates SoC of each agent can finally maintain consistency

delay. The consensus algorithm for interconnecting HESS units optimizes internal linkage efficiency via agent number and communication topology, enabling real-time state sharing, collaborative power distribution, and SoC equilibrium among batteries. Although the SoC can be stabilized within an approximate range, achieving exact convergence requires multiple adjustments. Additionally, line losses result in minor discrepancies between output and reference voltage. Future research will focus on validating the simulation model via small-scale hardware experiments and using hardware-in-the-loop (HIL) simulations, aiming to identify optimization potentials and formulate enhanced solutions for hardware-related challenges. Given the adaptability demonstrated by the proposed algorithm under signal delay and signal loss in simulation experiments, these hardware experiments are expected to operate robustly under fast-changing grid conditions while preserving real-time responsiveness.

CRediT authorship contribution statement

Tuohan Xiao: Writing – original draft, Validation, Software, Resources, Data curation, Conceptualization. **Don Gamage:** Writing – review & editing, Supervision, Conceptualization. **Chathura Wanigasekara:** Writing – review & editing, Supervision. **Akshya Swain:** Writing – review & editing, Supervision, Methodology, Conceptualization. **Abhishek Ukil:** Writing – review & editing, Project administration.

Declaration of competing interest

The authors declare that there are no conflicts of interest related to this study. All authors have disclosed any potential financial or personal relationships that could influence the research presented in this manuscript.

Data availability

Data will be made available on request.

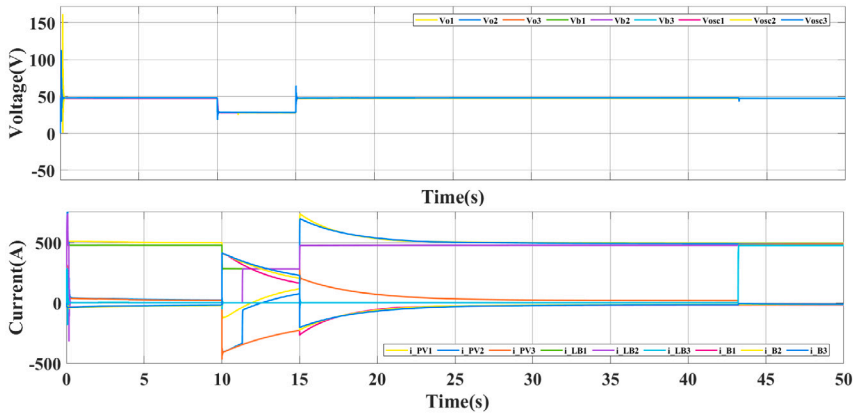

(a) Voltage and current curves of batteries and SCs.

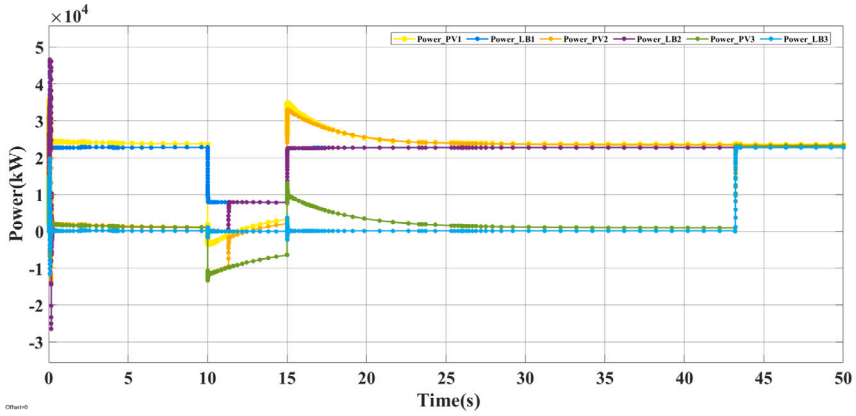

(b) Power curves of batteries.

Fig. 16. Output curves under advanced SVR controller.

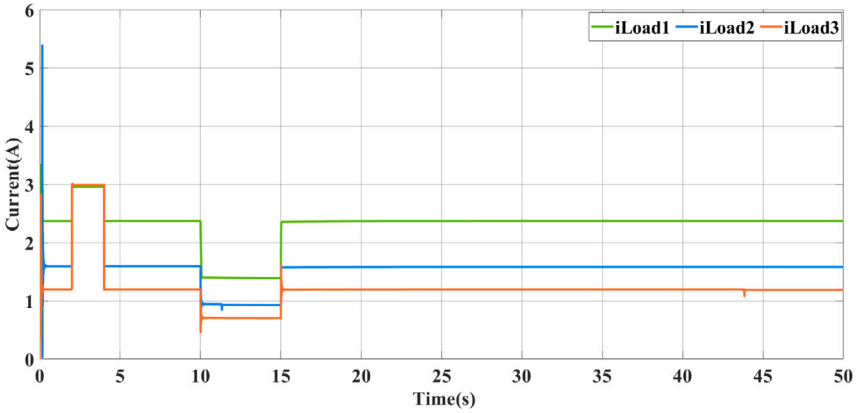

Fig. 17. Current of the load.

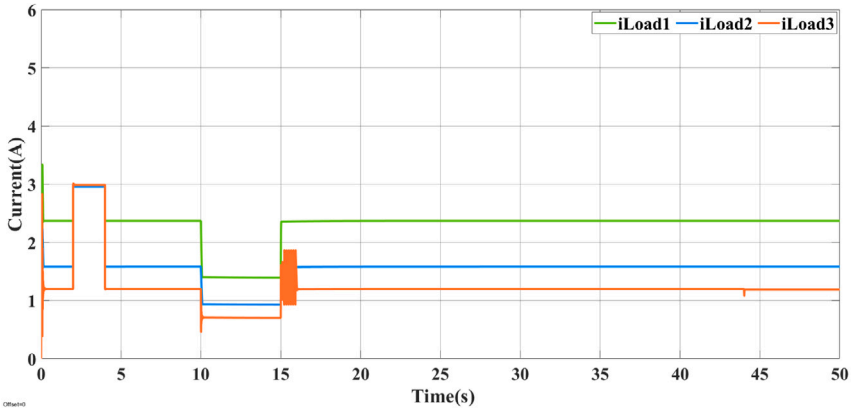

Fig. 18. Current of load while signal loss.

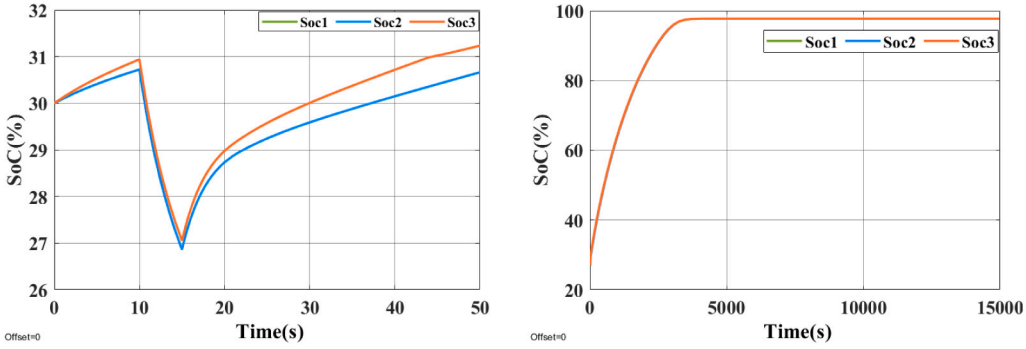

(a) First 50s of SoC charging. (b) Overall process of SoC charging.

Fig. 19. SoC while signal loss.

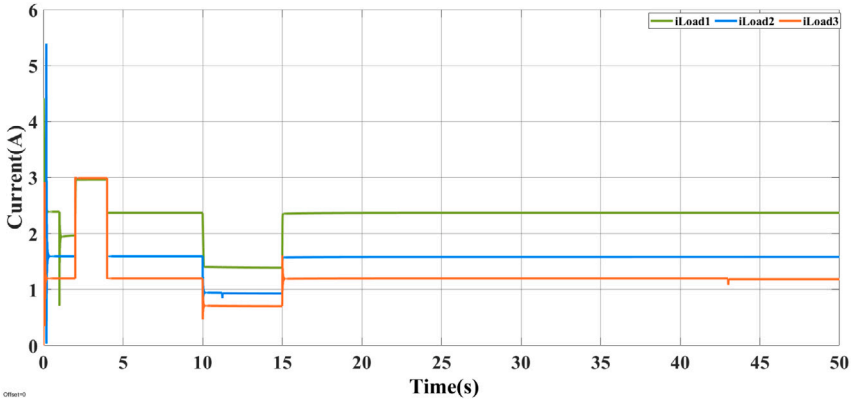

Fig. 20. Current of load while signal delay.

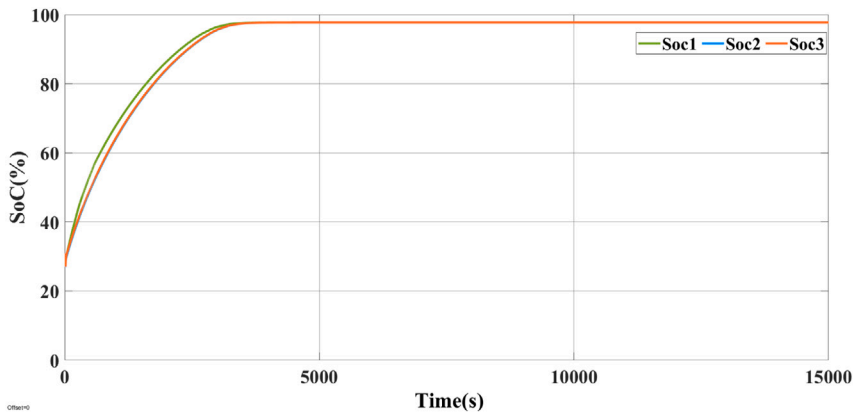

Fig. 21. SoC while signal delay.

References

[1] Kaoud Omar G, Elbassoussi Muhammad H, Zubair Syed M. Optimizing hybrid renewable energy systems for urban sustainability: A case study of five Saudi Arabian cities. Renew Energy 2025;123091.

[2] Gamage Don, Zhang Xibeng, Ukil Abhisek, Wanigasekara Chathura, Swain Akshya. Distributed co-ordinated consensus control for multi-energy storage of DC microgrid. In: 2021 IEEE power & energy society general meeting. PESGM, IEEE; 2021, p. 1–5.

[3] Ma Su, Liu Lu, Cheng Haozhong, Zhang Xiaohu, Xu Ling, Lou Wei, Wu Jiechen. Transmission grid and distribution grid flexible planning under high level renewable energy. Electr Power Syst Res 2025;245:111639.

[4] Shi Mengxuan, Chen Xia, Zhou Jianyu, Chen Yin, Wen Jinyu, He Haibo. Advanced secondary voltage recovery control for multiple HESSs in a droop-controlled DC microgrid. IEEE Trans Smart Grid 2018;10(4):3828–39.

[5] Pires VF, Pires A, Cordeiro A. DC microgrids: Benefits, architectures, perspectives and challenges. Energ 2023;16:1217.

[6] Pires V Fernão, Cordeiro Armando, Roncero-Clemente Carlos, Rivera Sebastian, Dragičević Tomislav. DC–DC converters for bipolar microgrid voltage balancing: A comprehensive review of architectures and topologies. IEEE J Emerg Sel Top Power Electron 2022;11(1):981–98.

[7] Gerber Daniel L, Vossos Vagelis, Feng Wei, Marnay Chris, Nordman Bruce, Brown Richard. A simulation-based efficiency comparison of AC and DC power distribution networks in commercial buildings. Appl Energy 2018;210:1167–87.

[8] Aljafari Belqasem, Vasantharaj Subramanian, Indragandhi Vairavasundaram, Vaibhav Rhanganath. Optimization of DC, AC, and hybrid AC/DC microgrid-based IoT systems: a review. Energ 2022;15(18):6813.

[9] Gamage Don, Wanigasekara Chathura, Ukil Abhisek, Swain Akshya. Multi-level consensus based load frequency controller with multi-battery energy storage systems. Electr Power Syst Res 2025;239:111208.

[10] Zhang Tongmao, Wang Xiao, Parisio Alessandra. A corrective control framework for mitigating voltage fluctuations and congestion in distribution networks with high renewable energy penetration. Int J Electr Power Energy Syst 2025;165:110508.

[11] Zhong Wei-Song, Dimirovski Georgi M, Zhao Jun. Decentralized synchronization of an uncertain complex dynamical network. In: 2007 American control conference. IEEE; 2007, p. 1437–42.

[12] Xu Qianwen, Xiao Jianfang, Wang Peng, Pan Xuewei, Wen Changyun. A decentralized control strategy for autonomous transient power sharing and state-of-charge recovery in hybrid energy storage systems. IEEE Trans Sustain Energy 2017;8(4):1443–52.

[13] Narendra KS, Oleng N, Mukhopadhyay S. Decentralised adaptive control with partial communication. IEE Proc, Control Theory Appl 2006;153(5):546–55.

[14] Xu Qianwen, Hu Xiaolei, Wang Peng, Xiao Jianfang, Tu Pengfei, Wen Changyun, Lee Meng Yeong. A decentralized dynamic power sharing strategy for hybrid energy storage system in autonomous DC microgrid. IEEE Trans Ind Electron 2016;64(7):5930–41.

[15] Sarić Aleksandar A, Khan Usman A, Stanković Aleksandar M. A distributed knowledge method for multi-agent power flow analysis based on consensus algorithms. Int J Electr Power Energy Syst 2024;162:110212.

[16] Gamage Don, Wanigasekara Chathura, Ukil Abhisek, Swain Akshya. Distributed consensus controlled multi-battery-energy-storage-system under denial-of-service attacks. J Energy Storage 2024;86:111180.

[17] Li Hongyi, Hui Hongxun, Zhang Hongcai. Consensus-based coordination of battery energy storage systems for frequency regulation service. In: 2023 IEEE 7th conference on energy internet and energy system integration. EI2, IEEE; 2023, p. 4768–73.

[18] Kang Wenfa, Chen Minyou, Guan Yajuan, Tang Liangchun, Guerrero Josep M, et al. Distributed event-triggered optimal control method for heterogeneous energy storage systems in smart grid. IEEE Trans Sustain Energy 2022;13(4):1944–56.

[19] Jiang Quanyuan, Hong Haisheng. Wavelet-based capacity configuration and coordinated control of hybrid energy storage system for smoothing out wind power fluctuations. IEEE Trans Power Syst 2012;28(2):1363–72.

[20] Kamel Rashad M, Chaouachi Aymen, Nagasaka Ken. Three control strategies to improve the microgrid transient dynamic response during isolated mode: A comparative study. IEEE Trans Ind Electron 2012;60(4):1314–22.

[21] Ecker Madeleine, Gerschler Jochen B, Vogel Jan, Käbitz Stefan, Hust Friedrich, Dechent Philipp, Sauer Dirk Uwe. Development of a lifetime prediction model for lithium-ion batteries based on extended accelerated aging test data. J Power Sources 2012;215:248–57.

[22] Bai Yunfei, Li Jianwei, He Hongwen, Dos Santos Ricardo Caneloi, Yang Qingqing. Optimal design of a hybrid energy storage system in a plug-in hybrid electric vehicle for battery lifetime improvement. IEEE Access 2020;8:142148–58.

[23] Kurzweil Peter, Schottenbauer Josef, Schell Christian. Past, present and future of electrochemical capacitors: Pseudocapacitance, aging mechanisms and service life estimation. J Energy Storage 2021;35:102311.

[24] Guo Jiaxin, Ping Ping, Ren Jinyong, Ren Xiantong, Gao Wei, Kong Depeng, Wang Dan, Feng Zhenkai. High-temperature calendar aging at low state-of-charge: Electrochemical degradation, thermal safety implications, and optimal SOC ranges for lithium-ion battery storage and transport. J Energy Storage 2025;125:116988.

[25] Jouili A, Boussaid B, Zouinkhi A, Abdelkrim MN. Finite time consensus for multi-tricycle systems under graph theory. In: 2020 20th international conference on sciences and techniques of automatic control and computer engineering. STA, IEEE; 2020, p. 24–9.

[26] Zhang Hongwei, Lewis Frank L, Das Abhijit. Optimal design for synchronization of cooperative systems: state feedback, observer and output feedback. IEEE Trans Autom Control 2011;56(8):1948–52.

[27] Chen Chi-Tsong. Linear system theory and design. Saunders college publishing; 1984.

[28] Khazaei Javad, Miao Zhixin. Consensus control for energy storage systems. IEEE Trans Smart Grid 2016;9(4):3009–17.